University of Thessaly

Department of Mechanical Engineering

Numerical Simulation of the Pulsations of a Broken Contrast Agent Microbubble

By

Chatzigeorgiou Eleni

Supervisor Prof. N. Pelekasis

Submitted in partial fulfillment of the requirements for the Diploma of Mechanical Engineering

July 2018

Abstract

Ultrasound imaging is an important part of modern diagnostics and therapeutics in Medicine. Even though ultrasound has been a significant asset to the medical science for almost a century, there is still need for improvement when it comes to the production of a clear image of the targeted object. For this reason, a large number of studies is focused on the investigation and manufacturing of several types of microbubbles to be used as contrast enhancement agents. The properties of the microbubbles and their behavior, when they are under the influence of an ultrasound acoustic signal, make them promising contributors to the ultrasound imaging methods as diagnostic tools. Additionally, these contrast agents have the potential to be used as carriers for specifically targeted drug and gene delivery treatments. This also attributes to their abilities when they are insonified that stem from the properties of their coating and the encapsulated gas. It has been observed that when contrast agent microbubbles exist in a liquid environment and are under the influence of an acoustic signal, they pulsate due to the elasticity of their shell material and they can also break if the insonification signal is intense enough. The assets that these microbubbles have to offer to the medical science make them especially worthy of research. Therefore, it is important to observe, record and understand the mechanics behind their behavior when they are being insonified, to the extent that they can be manipulated to fulfill any presented need. It is particularly meaningful to evaluate if and how these coated microbubbles can be useful when they are damaged as well as when they are intact.

In the present diploma thesis, a numerical analysis of the behavior of a single pulsating microbubble based on the Kelvin-Voigt model for small displacements is performed. FORTRAN code serves as the computational environment for the simulation. The problem involves a coated microbubble that is placed in an aqueous environment and undergoes pulsations as a result of an ultrasound acoustic signal and consists of two consecutive parts. In the first part, the microbubble is simulated to be intact while oscillating, while in the part that follows, the microbubble is considered broken and part of the gas that it contained has escaped and formed a smaller pulsating microbubble. The connection between the two parts of the problem is made through a parametric analysis that provides the initial values for the simulation of the broken microbubble part of the problem. The results of the simulation are being compared to optical observations of an experimental representation of the same problem. After observation of the available results, it could be concluded that it is possible to identify the condition of a microbubble existing in an aqueous environment by the root-mean-square (RMS) of the scattered pressure and the scattering cross section. Further research was found to be necessary in order to accurately describe the behavior of a broken pulsating microbubble with a mathematical model.

Table of Contents

List of Figures

List of Tables

Table of variables

MI	Mechanical Index
PNP	Peak Negative Pressure
F_c	Center frequency of the ultrasound wave
R_0	Initial radius of the microbubble shell (before insonification)
ω_f	Frequency of the acoustic signal
ρ_l	Density of the surrounding liquid
R_{sh}	Radius of the microbubble shell
R_f	Radius of the free gas microbubble
P_{gas}, P_g	Pressure of the encapsulated gas
P_{liquid}	Pressure of the surrounding liquid
P_{stat}, P_{st}	Static pressure
μ_l	Dynamic viscosity
G	Stress modulus
P_{AC}	Pressure of the acoustic signal
P_∞	Pressure of the liquid away from the microbubble
M	Mach number
$\dot{R}$	Microbubble-liquid interface velocity
$\ddot{R}$	Microbubble-liquid interface acceleration
$P_{l_{r=R}}$	Pressure of the surrounding liquid on the surface of the microbubble
We	Weber number
Re_l	Reynolds number of the surrounding liquid
u	Microbubble shell displacements
$dist$	Distance between the microbubble and the position of the acoustic signal transmitter
$P_{scattered}$	Scattered pressure signal
V	Volume of the microbubble
scs	Scattering cross section
$P_{sc,RMS}$	Root mean squared scattered pressure

Acknowledgements

I would first like to express my gratitude to my thesis supervisor Professor N. Pelekasis for providing me with the opportunity to work on a subject that I was very interested in and guiding me throughout the time of my study. The door to Prof. Pelekasis office was always open whenever I ran into a trouble spot or had a question about my research or writing and that was greatly appreciated.

I would also like to express my appreciation to Dr. K. Efthymiou for his help with the understanding of the preexisting FORTRAN code and the basics of the problem. In addition, I would like to thank the other members of the Fluid Mechanics Laboratory for their support and encouragement, as well as, for their willingness to help at any time.

I would like to thank Professor V. Bontozoglou and Assistant Professor G. Charalampous for taking the time to serve as my thesis committee and for reading my thesis.

I am thankful for the lifelong friends that I made in my years studying in Volos and the amazing times that we spent together and especially to Vaso for taking care of me in times of pressure. I am also thankful for my childhood friends, Despina, Natasa and Tasos, who continued to love and support me all these years that I was away. I feel privileged to have people in my life that I can look up to and urge me to be better every day. I would like to give special thanks to my friend Kleanthis for always being willing to help me with any technical issues that I faced while writing this thesis. I also greatly appreciate Margianna for her emotional support all these years, for setting the bar as high as possible with her example and for constantly pushing me to do better.

Τέλος, θα ήθελα να ευχαριστήσω θερμά τους γονείς μου χωρίς των οποίων την υποστήριξη και την συμπαράσταση η φοίτησή μου σε αυτή τη σχολή δεν θα ήταν δυνατή, και στους οποίους αφιερώνω αυτή την εργασία.

1. Introduction

The need to discover and understand the way the human body works has been present from the beginning of civilization. As the medical science developed and continued to progress, the opportunity to obtain an image of what is inside the human body was possible. In order for doctors to progress further in their medical achievements, ultrasound imaging became an important asset and the improvement of this method became of vast importance. One way that ultrasound imagining could be improved was with the assistance of microbubbles as contrast agents.

"Contrast agents are a category of microbubbles filled with gas, usually soluble in blood, enveloped in a membrane or polymer shell. They are primarily used to enhance ultrasound imaging or for targeted drug delivery." [1]

Contrast agent microbubbles have been in the forefront of medically related research for the past couple of decades, especially focusing on contrast ultrasound imaging methods and targeted drug/gene delivery. Their volumetric oscillations when subjected to an acoustic signal are the reason behind their ability to enhance the ultrasound imaging. [2] In the first case, of ultrasound imaging enhancement, the selection of a suitable gas core is of utmost importance because it determines the echogenicity; the ability of the bubble to reflect a characteristic echo, when caught in an ultrasonic frequency field. Gasses that can be used in the composition of a contrast agent are air or other heavier options, like perfluorocarbon or nitrogen, which help in the prevention of leakage and, eventually, dissolution of the bubble. In the second case of drug delivery, the most important is the selection of the shell material, which determines how easily the microbubble is taken up by the immune system. More hydrophilic materials tend to be absorbed more easily, therefore the time available for the contrast imaging is reduced. The fact that some materials can give the shell they compose the ability to rupture under a specific pressure makes those microbubbles an ideal carrier for specifically targeted treatment. Finally, the shell material's elasticity determines how long it can last before it bursts.

1.1. Characteristics of microbubbles

There is a variety of different microbubble types regarding their composition, properties and application. Each type of microbubble has its own unique advantages and can be tailored for specialized functions. In general, a microbubble comprises of a gas core, taking up the majority of its volume, and a shell with the purpose to stabilize the gas bubble when it exists in a liquid. The shell can be composed of surfactants, lipids, proteins, polymers, or a combination of the above. [3] A representation of a typical microbubble composition is provided in *Fig.1*. A more detailed presentation of the microbubble shell types follows.
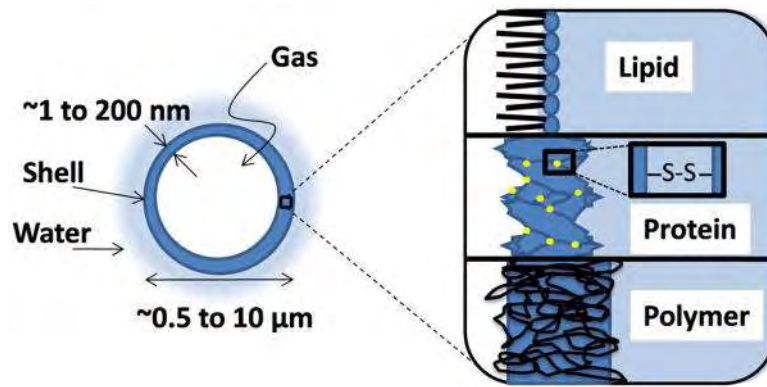
Figure 1 A representation of a typical microbubble with different shell compositions *[3]*

Protein shells

Within the category of protein shelled contrast agents there are the albumin shelled microbubbles, which were a pioneering formulation for this application at the time they were introduced. They were followed by several similar formulations with the ability to pass the lung capillaries and provide contrast in the left ventricle of the heart. Specifically, Albunex was the first albumin microbubble formulation to be approved by the US Food and Drug Administration (FDA). [4]

Other than albumin, several proteins are used to coat microbubbles due to their amphipathic nature, which makes them highly surface active. [3]

Surfactant shells

A substance which tends to reduce the surface tension of a liquid in which it is dissolved is called a surfactant. Mixtures of synthetic surfactants, like SPAN-40 and TWEEN-40, have been used by Wheatley et al. to stabilize contrast agents. [5] The microbubbles are created by sonicating the surfactant solution in the presence of air.

It was recently reported that stable microbubbles could be formed from sucrose stearate (mono- and di-ester). [6] These microbubbles were reportedly stable in suspension for over a year and portrayed unique domain morphology. The reason behind these achievements was the interaction between surface tension, domain boundary line tension and spontaneous curvature of the surfactant monolayer. These particular microbubbles were not stable upon dilution, thus they are not fit for biomedical applications. This study, though, indicated the importance of surface heterogeneity and domain bending on microbubble stability.

Lipid shells

This kind of microbubbles is considered as one of the most interesting and useful formulations used for biomedical imaging and drug delivery. [3] What is particularly interesting is the fact that the lipid shell was, in a way, a natural inspiration given that stable microbubbles that are found in every aquatic environment on Earth are known to be stabilized by acyl lipids and glycoproteins. [7] What is more, the lipid shell of these microbubbles mimics the stability and compliance of lung surfactant [8] which was discovered based on the observation of stable microbubbles formed from lung lavage. [9] Among the commercially available lipid shelled microbubbles there is Definity (Lantheus Medical Imaging), which was used by DH Thomas et al. in order to identify the occurrence of the microbubble's resonance in vivo. [2]

Lipid shells present a number of advantages owing to their hydrophobic/hydrophilic assembly and the forces that bind then together. Specifically, a lipid monolayer is formed spontaneously around a freshly appeared gas bubble, where the hydrophobic acyl chains face the gas core and the hydrophilic headgroups face the surrounding liquid. These lipid monolayers are highly cohesive, adding stability to the shell, [10] while the lipid molecules are "weakly" bound together due to the absence of chain entanglement, making the shell compliant to area expansion and compression. [3] As a result, this kind of microbubble contrast agents present favorable ultrasound characteristics.

Polymer shells

The term *polymer microbubble* typically refers to a type of microbubbles that are stabilized by a thick shell comprising of polymeric species, which make it more resistant to area compression and expansion. Polymer microbubbles have been observed to fracture during insonification, releasing their gas core through the shell defect. The polymeric shell also reduces the echogenicity and drug delivery activity. [11]

1.2. Applications

There is a variety of microbubble types and each of them can portray numerous useful properties when insonified by an ultrasound signal. [12] [13] These properties may depend on the ultrasound parameters, the microbubble size or its physicochemical composition. Different properties can be exploited for different medical purposes. For example, subtle effects like an acoustic backscatter can be utilized in diagnostic imaging, whereas more drastic effects like inertia cavitation can be used for targeted drug delivery. Between these two extreme forms of microbubble reactions there is a range of useful effects that can be exploited by modern ultrasound theranostics techniques. Some useful ultrasound-mediated effects of microbubbles for biomedical applications, other than acoustic backscatter and inertia cavitation, are streaming, fragmentation, dissolution and radiation force.

In more detail, *streaming* of the surrounding fluid creates shear forces that can assist in drug release from the microbubble and absorption from the nearby cells. *Fragmentation*, on the other hand, is caused by higher acoustic pressures and refers to the emergence of multiple microbubbles from the division of the original one. [14] It is a useful means of eliminating the contrast agent signal within the transducer focus. Microbubble fragmentation is being employed to measure reperfusion in tumor and cardiac tissue and in ultrasound molecular imaging methods. Insonification at moderate pressures below the fragmentation threshold results in *dissolution* of the gas core. Dissolution offers a more subtle means of eliminating the contrast signal and can also be useful for drug delivery. Finally, insonification at low pressures near microbubble resonance leads to *radiation force*, which displaces the microbubble away from the transducer. Radiation force may be used to move the microbubble to the preferred place inside a vessel, while a secondary radiation force may also be useful due to the fact that microbubbles oscillating in phase may attract each other, resulting in microbubble clumps that may significantly enhance the echogenicity and drug delivery capability. [15] [16]

The reason that microbubbles are considered to be the top contrast agent option for ultrasound imaging lies in their compressibility, which is the main factor behind their strong echogenicity. [16] [17]The primary interest for microbubbles is their utilization as contrast enhancement agents in one of the most accessible and safe imaging methods that is ultrasound imaging. Other than this practice, and molecular imaging, there is intensive research around the use of microbubbles as targeted delivery vehicles. The cavitation of the

microbubbles that occurs in an ultrasound field is a factor that contributes to the permeability of the cell plasma membrane and the local endothelial vasculature that is targeted, allowing small molecules or even larger ones, such as DNA, to be transferred through the blood stream into the specifically desired tissue. This technique is referred to as sonoporation. [18]

The mechanism that allows the carried drug to be absorbed after its release from the microbubble significantly affects the designing process of the microbubble carrier aiming to be a reasonable choice for drug delivery triggered by ultrasound. It is observed that the size and qualities of the delivered drug influence the means required to accomplice their delivery. There needs to be a balance between the intensity of the ultrasound burst and that of the cavitation imposed on the carrier microbubble.

A viable choice of contrast agent microbubble for in vivo imaging and molecular targeting is considered to be thick shelled polymer microbubbles filled with gas. Not enough research has been done on the matter, though, mostly because there are doubts concerning the efficiency of this type of coated microbubble in genes/drugs depositing mechanisms due to the shell's resistance to fragmentation. As a result, lipid or protein coated microbubbles have been preferred for this kind of process. However, a relatively recent study by Mehier-Humbert et al. has presented evidence that hard-shelled microbubbles, such as polymer coated ones, exhibit potential as ultrasound-mediated drug/gene delivery carriers. [19]

1.3. Literature

The idea of using these agents to achieve a clearer ultrasound image originally appeared by accident in the late 1960s. It was observed that by injecting agitated saline, a noticeable signal change occurred during an ultrasound examination. [20] The enhanced contrast appeared because of the compressible gas core of saline bubbles, which enabled the bubble to backscatter the applied ultrasound signal. [21]

It was only for the past few decades, though, that significant progress towards the development of microbubbles as *theranostics* on a wide variety of biomedical applications was made [3].Theranostics is a term very recently proposed to describe a combination of therapeutics and diagnostics. A more detailed definition, proposed in 2013, is the following:

"*Theranostics* is a proposed process of diagnostic therapy for individual patients to test them for possible reaction to taking new medication and to tailor a treatment plan for them based on the test results." [22]

The development of more stable bubbles with sufficient lifetime and a clearly defined size took more than 20 years from the time they were first discovered. The first such bubble was Albunex®, a commercially available ultrasound contrast agent that comprised an albumin shell and an air filled core. [23]

More recently, Bjerknes et al. (1997) were able to describe a method for the creation of microbubbles but with a very broad size distribution of 1-20μm. It was observed that this kind of microbubbles had an elongated, crumpled shape. It also became apparent, via acoustic tests, that there was a dose-dependent increase in acoustic attenuation. [24]

The next breakthrough in the investigation of microbubbles came shortly after, in 1999, by Narayan and Wheatley who reported on microbubbles formed by a biodegradable copolymer

called PLGA. [25]These microbubbles were made hollow with the use of a volatile solid core that had the ability to be taken away. Their size distribution also ranged from 2-20μm in diameter. An interesting fact was that they were able to observe significant ultrasound contrast in the right kidney of rabbits, which showed that a large population of the injected microbubbles was able to pass through the lung capillaries which typically restrict particle with a diameter greater than 10μm.

The fabrication of the same type of microbubbles was described by Cui et al. in 2005 with a double emulsion, solvent evaporation method. Their size distribution was showed to be between $1 - 2\ \mu m$ in diameter and their shape was observed to be spherical with smooth surfaces without visible pores and cavities. These PLGA microbubbles filled with either air or perfluoropropane (PFB) were capable of opacifying the left ventricle (LV) due to their diameter distribution. [26]

In the same year, Cavalieri et al. described a method to create a different type of microbubbles, coated with poly (vinyl alcohol) or PVA. These microbubbles had a self-life of several months and were capable of carrying hydrophobic drugs, charged molecules like DNA and targeting ligands. [27]

In 2006, Böhmer et al. described a new method of creating polymer microbubbles using ink-jet printing. These microbubbles, called PLA-PFO (polyperfluorooctyloxycaronyl-poly or lactic acid), were created by injecting an organic phase containing the polymer into an aqueous solution. An additional non-solvent for the polymer was used to create the core/shell morphology, and the core was removed to create the hollow chamber. [3] [28]

Another polymer shelled microbubble type called PB-127 has been developed, that consists of a polymer/albumin shell and a nitrogen core and it is effective for intermittent harmonic power Doppler imaging. It is used as an ultrasound imaging agent for assessing myocardial perfusion on patients with coronary artery disease. [29] Bouakaz et al. conducted optical observations on PB-127 type microbubbles of various sizes in order to determine a pattern of oscillation when they are under the influence of an acoustic signal. [30] The experimental procedure that was followed during the investigation is described below.

A microbubble consisting of a polymer/albumin shell and a nitrogen gas core was inserted in a liquid environment. A transmitter was placed in a distance of $75mm$ from the position of the bubble. The transmitter emitted a 10 cycle acoustic signal of $1.7MHz$. The microbubble, after receiving the signal, began to oscillate. After a certain amount of time the microbubble was observed to rupture [30], releasing part of the gas existing in its core. The pulsations continued to occur, as the acoustic signal was then applied on a system of the polymer/albumin shelled microbubble and a newly formed free gas microbubble. The free gas microbubble eventually dissolved.

The experimental observations that were carried out were divided into three categories based on the mechanical index (MI) used as a form of quantification of the applied acoustic pressure; low MI, medium MI and high MI insonification.

The mechanical index in relation to the acoustic pressure is defined as follows:

$$MI = \frac{PNP}{\sqrt{F_c}}$$
[1]

Where PNP stands for Peak Negative Pressure of the ultrasound wave in MPa and F_c is the center frequency of the ultrasound wave in MHz [31]

After the observation of the pulsations of several insonified microbubbles in a variety of sizes with a 10 cycle and $1.7MHz$ frequency ultrasound signal, the following graph was created. Fig.2 categorizes the behavior of a microbubble according to its diameter and the MI of the acoustic signal imposed on it. The observed data are divided into three categories: the non-destruction zone, the transient zone and the destruction zone. The non-destruction zone contains the microbubbles that either have small diameters or are insonified with a low MI signal. These microbubble pulsate throughout the insonification without breaking. The destruction zone involves microbubbles with a large diameter regardless of the MI of the acoustic signal or microbubbles with a relatively small diameter (as low as $3.5\mu m$) but with an insonification signal of a MI more than 0.7.
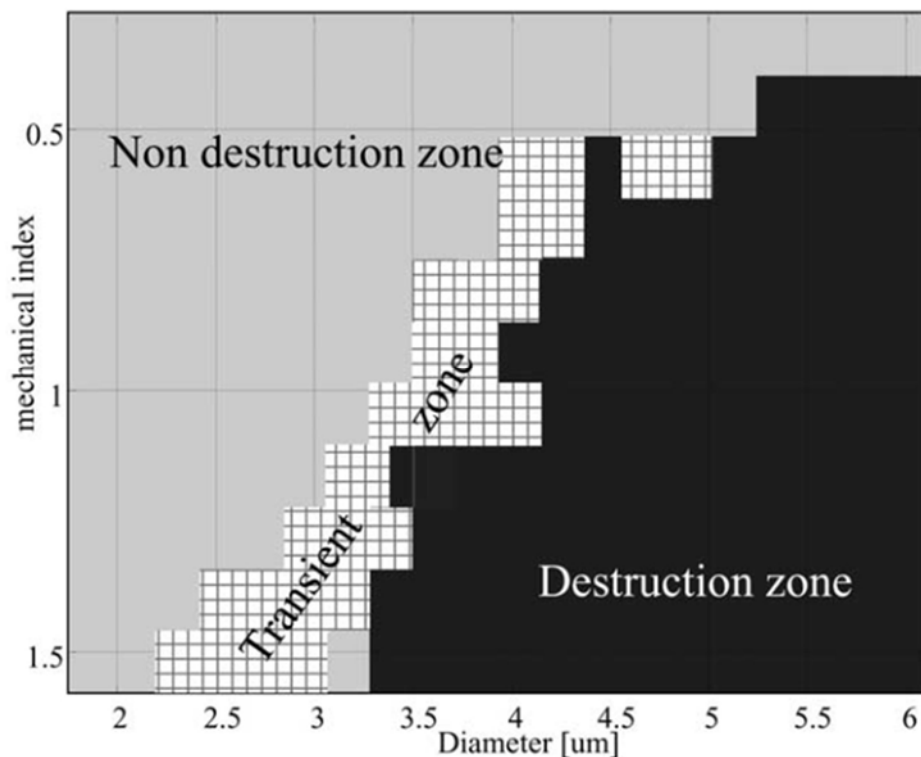
Figure 2 Response of PB127 microspheres as a function of their initial size and applied mechanical index [30]

In situations similar to the experimental setting where the observations about the behavior of the oscillating microbubble were made, there is also the phenomenon of diffusion taken into account. Specifically, when the observations involve a spherical oscillating bubble that remains in place during the pulsations, the part of the observed space that is affected by the phenomenon of diffusion is a thin layer in the area of the dynamic gas-liquid interface. The mass transport through that layer though could potentially result to a measurable difference on the volume of the bubble. The gas bubble could either dissolve into the surrounding liquid or, as is the case with rectified diffusion, increase in mass if the volume oscillations that the bubble undergoes are intense enough. [32] Research on how much this phenomenon affects the behavior of a pulsating bubble has been done by Fyrillas & Szeri with the development of a new theoretical formulation. [33] The results of this research state that the part of the

diffusion that accounts for the oscillatory behavior of the bubble contributes very little to the mass transport in the first few periods of oscillation and can be neglected asymptotically in time. That is attributed to the very fast timescale of the oscillations in comparison to the timescale of the mechanism of diffusion. [33] As a result, diffusion of the gas core into the surrounding liquid is neglected during this study.

2. Methodology

The potential use of polymer coated microbubbles in drug delivery processes and their already proven efficiency in ultrasound image enhancement is providing motive for further research on their full range of abilities and behaviors when under the influence of an acoustic signal. More specifically, it is intriguing to investigate a gas filled microbubble's response to an acoustic signal in relation to its rupture, assisting both prominent applications; ultrasound imaging and drug delivery.

It would be very useful to be able to differentiate the backscatter signal of an intact pulsating microbubble from that of a microbubble that has been broken and continues to pulsate. This information would help recognize when a carrier microbubble, for example, has delivered the contained drug successfully to the targeted area or whether a microbubble can be useful as a contrast enhancement agent even after its shell has broken.

The objective of the present thesis is to investigate if the reaction of a coated microbubble to an acoustic signal can be simulated via the mathematical equations described in subsection 2.2 entitled *Problem Formulation*. It is attempted to simulate the behavior of a microbubble under the influence of an acoustic signal, in an intact and a broken state, and compare the results to the data provided by optical observations that exist on the matter. The conditions on which the simulation is based are the ones under which a set of experimental optical observations by Bouakaz et al. takes place [30] and are described in more detail in *Problem Formulation*. The main aim is to see whether the optical observations of a pulsating microbubble can be duplicated and explained adequately by the mathematical model presented.

The microbubble being investigated is coated with a polymer shell and contains gas that is considered to be ideal. An acoustic signal is emitted by a transmitter placed in a distance of $75mm$ from the position of the microbubble. The signal is characterized by a 10 cycle duration and a $1.7MHz$ frequency. When the signal reaches the microbubble, it inflicts oscillations. After a couple of pulsations, the microbubble's shell brakes due to the stresses induced on the shell material. The rupture occurs at a point in time right before the point of maximum expansion of the selected cycle. The breach on the microbubble's shell allows the encapsulated gas to escape and form a free (uncoated) gas microbubble, approximately one tenth of the initial microbubble's size. For as long as the acoustic signal continues to be transmitted, the broken microbubble shell continues to oscillate along with the free gas microbubble that has just formed. During the contraction of the microbubble, the free gas bubble is observed to disappear inside the matrix microbubble, while it comes out again when the microbubble shell is in a state of expansion. This behavior continues until the end of the insonification.

2.1. Nondimensionalization

All the variables used in the equations governing the problem have been converted into dimensionless. In order to nondimensionalize the variables, appropriate units were used for each one of them. The characteristic values are displayed in the *Table I* below.

Table I Nondimensionalization characteristic values

Variable	Characteristic value
Radius	R_0
Time	$1/\omega_f$
Velocity	$\omega_f R_0$
Pressure	$\rho_l \omega_f^2 R_0^2$

The fact that dimensionless values were used throughout the numerical solution of the problem makes the results applicable to any microbubble following the same procedure, when the corresponding data are inserted as input.

2.2. Problem formulation

The problem being considered consists of two consecutive parts; the intact microbubble problem and the broken microbubble problem. A schematic representation of the former is presented in *Fig.3*. The equations governing each of the individual parts are similar, in the sense that they are essentially describing the same problem type (the oscillation of a microbubble). The main difference lies in the quality and the conditions of the microbubble-surrounding liquid interface, specifically the existence or not of an encapsulating material, and the size of the microbubble. A transitional part including a parametric study exists, in order to provide the broken microbubble problem with the optimal moment of fracture and the conditions that it involves.
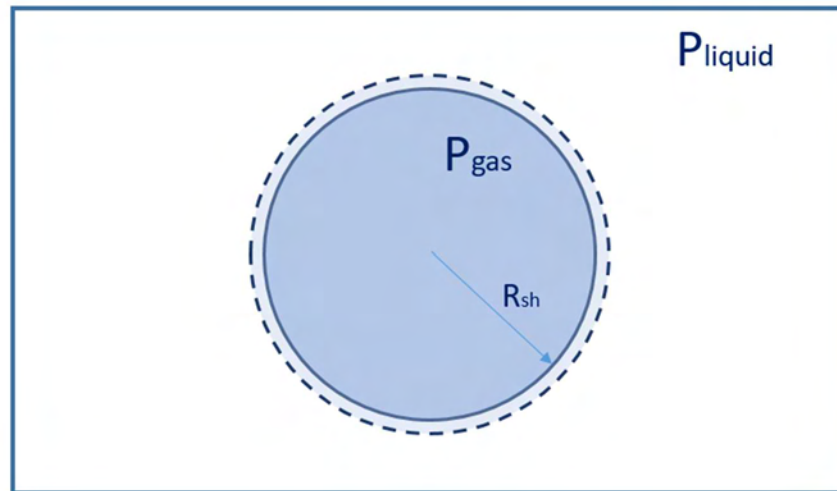
The intact microbubble problem

Figure 3 Depiction of the oscillating microbubble during the first part of the problem

In the first part, the microbubble, which is submerged in a liquid, is exposed to an acoustic signal of 10 cycles and a 1.7MHz frequency and appears to oscillate expectedly while its shell remains intact. The mechanical index of the imposed acoustic signal is taken equal to 0.6 in accordance with the data provided by optical observations [30]. The oscillations continue to occur for as long as the insonification of the microbubble happens.

Assumptions

Before the simulation took part some necessary assumptions were made in order to simplify the calculations that needed to be made.

- The oscillations of the polymer shelled microbubble were considered to be spherosymmetric.
- The effects of inertia on the shell were neglected.
- The external environment of the bubble was considered to be a Newtonian liquid and the internal gas to be ideal.
- We investigated the behavior of a single microbubble in an aqueous environment. There is sizeable difference in the behavior of a larger number of microbubbles under the influence of an acoustic signal due to a variety of mutual interactions between the microbubbles.
- Isothermal changes are assumed throughout the problem.
- Residual stresses on the microbubble shell were neglected.

Initial conditions

The initial conditions for the first part were assumed according to the results provided from the optical observations made by Bouakaz et al. [30].

The microbubble radius chosen for the investigation was taken to be $2\mu m$ (or alternatively a $4\mu m$ diameter). The density of the surrounding liquid was taken equal to the density of water ($998 Kg/m^3$).

Based on a set of experimental data [34] and various other experimental and theoretical studies regarding contrast agents the following values were obtained.

A range between 0.6 and $1.6 Pa*s$ is suggested for the dynamic viscosity. $1Pa$ is the final chosen value.

The shear stress modulus is allowed a variation between 35 and 105 MPa for lipid shelled microbubbles. [35] Considering that the microbubble in this study was a polymer shelled one, the chosen value for the shear stress modulus was higher, at $200MPa$.

The shell thickness was considered to be $15nm$ and remaining the same throughout the investigation. [35]

The amplitude of the imposed acoustic signal was taken equal to $8MPa$ based on *Eq.1* and the fact that the investigated MI and frequency of the problem were 0.6 and $1.7MHz$ respectively and *Eq.2* for static pressure equal to $1atm \approx 0.1013MPa$.

Governing equations

The sinusoidal pressure disturbance applied on the bubble is of the following form [35]:

$$P_\infty\left(t\right) = P_{stat} + P_{AC} = P_{stat}\left[1 + \varepsilon\sin\left(\omega_f t\right)\right] \tag{2}$$

with the forcing frequency lying in the regular ultrasound range.

The same pressure disturbance is applied throughout both parts of the problem and is presented in *Fig.4*.

The microbubble's shell follows Kelvin-Voigt (KV) constitutive law which is Hooke's law for incompressible materials and relates the viscoelastic stresses to the strain and strain rate tensors in a linear manner. The oscillation resulting from the exposure of the microbubble to the acoustic signal is described by the following equation, which is essentially the Keller-Miksis (1980) model for radial oscillations and describes spherosymmetrical oscillations in a compressible fluid [35]:

$$\left(1 - M\dot{R}\right)R\ddot{R} + \left(\frac{3}{2} - \frac{M\dot{R}}{2}\right)\dot{R}^2 = \left(1 + M\dot{R}\right)\left(P_{l_{r=R}} - P_{st} - P_{AC}\right) + MR\frac{d}{dt}\left(P_{l_{r=R}} - P_{AC}\right) \tag{3}$$

Mach number is small but not negligible: $M = \omega_f R_0/c$

R: undimensional external microbubble radius
$\dot{R}$: velocity of external microbubble radius
$\ddot{R}$: acceleration of external microbubble radius
$P_{l_{r=R}}$: dimensionless pressure of the surrounding liquid
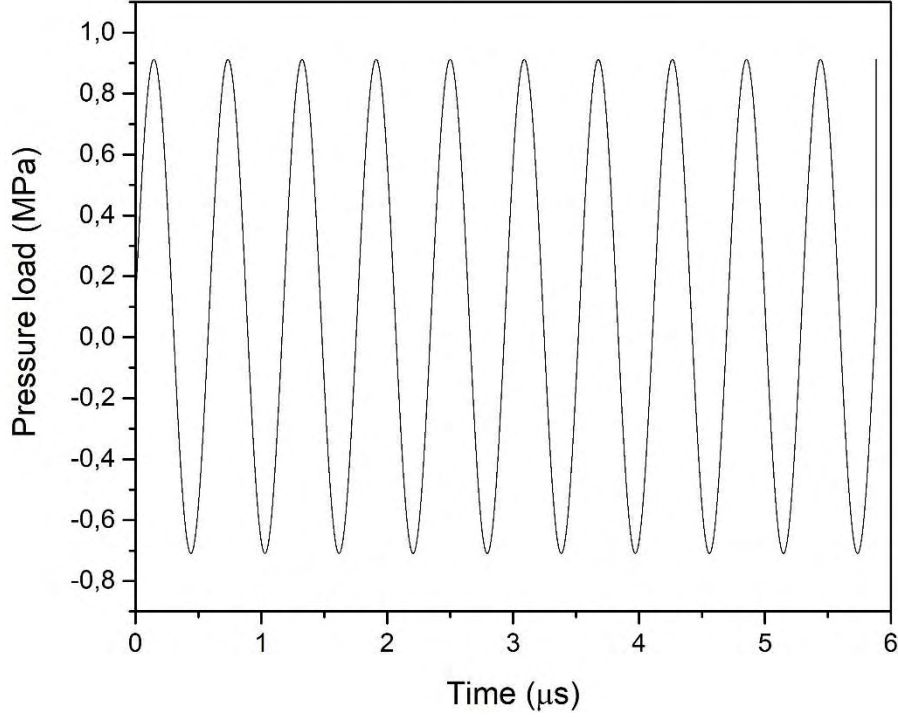
Figure 4 Pressure disturbance of applied acoustic signal

The pressure of the surrounding liquid is described by the following equation:

$$P_{l_{r=R}} = \left[\frac{2}{We} + P_{stat}\right]\left(\frac{1}{R}\right)^{3\gamma} - \frac{2}{WeR} - \frac{4}{Re_l}\frac{\dot{R}}{R} - \frac{4m}{Re_l}\frac{\dot{R}}{R^2} - 2\frac{3G}{R}\left(\frac{R^2}{(1-u)^2} - 1\right) \qquad [4]$$

deriving from the stress equilibrium between the membrane, the external liquid and the internal gas.

Variable u represents microbubble shell displacements. Residual stresses on the microbubble shell were neglected, therefore $u = 0$.

The scattered pressure signal that is received at the position of the transmitter of the initial acoustic signal is described by $Eq.\,5$ [36] [2].

$$P_{scattered} = \frac{R_{sh}^2}{dist}\ddot{R}_{sh} + \frac{2R_{sh}}{dist}\dot{R}_{sh}^2 - \left(\frac{R_{sh}}{dist}\right)^4\frac{\dot{R}_{sh}^2}{2} \qquad [5]$$

Where $dist$ is the distance between the position of the microbubble and that of the transmitter, where the signal is received, and is taken equal to $75mm$.

The equation correlating the gas pressure to the volume of the microbubble (*mass conservation*):

$$P_g{'}V{'}^\gamma = P_{g,0}{'}V_0{'}^\gamma \qquad [6]$$

where $\gamma = 1.07$ and subscript 0 denotes the initial status before the beginning of the pulsations.

The dimensionless numbers involved in the previous equations have the form noted below:

$$We = \rho_l \omega_f^2 R_0^3 / \sigma$$
$$Re_l = \rho_l \omega_f^2 R_0^2 / \mu_l$$
$$m = 3\mu_s \delta / \mu_l R_0$$
$$G = \delta G_s / \rho_l \omega_f^2 R_0^3$$

[7]

The scattering cross section of the backscattered signal from the oscillating microbubble is given in $Eq.\,8$. [35]

$$scs = 4\pi \frac{\int_0^{t_f} dist^2 P_{scattered} \, dt}{\int_0^{t_f} P_{AC}^2 \, dt}$$

[8]

The RMS scattered pressure is given in $Eq.\,9$ [2]:

$$P_{sc,RMS} = \sqrt{c_0^2 + \sum_{n=1}^{\infty} \frac{|c_n|^2}{2}}$$

[9]

Where c_0, c_n are coefficients related to the scattered pressure Fourier series of $Eq.\,10$.

$$P_{sc}(t) = \sum_{n=-\infty}^{\infty} c_n e^{-i(2n\pi/\Delta t)t}$$

[10]

Transition to the broken microbubble problem

Due to the stresses that were imposed onto the elastic shell of the microbubble during its pulsation, a breach occurs on the material. That allows the gas that was encapsulated in the microbubble to escape and form another smaller microbubble that is attached onto the initial one at the point of rupture. The insonification continues and affects both microbubbles that exist now.

Two new variables are introduced in the formulation of the problem in order to model the pulsations of the free gas microbubble that has occurred; the radius of the free microbubble (R_f) and its velocity ($\dot{R}_f$). The radius of the new gas bubble is initially assumed to be approximately one tenth of the current radius of the microbubble shell. In order to calculate the initial free gas bubble radius velocity, a parametric study was employed with the assistance of a *Matlab* algorithm, with the moment of the rupture and the value of the free microbubble radius as independent variables. The data connected to the moment of the rupture that are necessary for carrying out the following equations are the microbubble shell and the pressure of the surrounding liquid. The equations that ultimately resulted to the final choice of the two variables' values where the following:

$$We = \frac{\rho_l \omega_f^2 R_0^3}{\sigma}$$

[11]

$$Re_l = \frac{\rho_l \omega_f^2 R_0^2}{\mu_l}$$

[12]

21

$$P_{stat_d} = \frac{P_{inf}}{\rho_l \omega_f^2 R_0^2} \tag{13}$$

$$P_{l_d} = \frac{P_l}{\rho_l \omega_f^2 R_0^2} \tag{14}$$

$$P_{g_d} = P_{g,0} \left[\frac{1}{R_f^3 + R_{sh}^3} \right]^\gamma \tag{15}$$

which is the dimensionless mass conservation equation for the microbubble shell and the free gas bubble

$$\dot{R}_{b_d} = \frac{Re_l}{4} R_{b_d} \left[P_{stat} \left(\frac{1}{R_{b_d}^3 + R_{shell_d}^3} \right)^\gamma - P_{l_d} \right] - \frac{2}{We} \tag{16}$$

$$\dot{R}_b = \dot{R}_{b_d} \, \omega_f R_0 \tag{17}$$

where subscript *d* stands for *dimensionless* values.

The equations that describe the oscillation of the microbubble shell and free gas bubble system are similar to the first part of the problem but adjusted to the existence of two different radii. More specifically, the mass conservation equation obtains the dimensionless form portrayed in $Eq. 15$.

The equation correlating the radius velocity of the microbubble to the pressure difference between the encapsulated gas and the surrounding liquid is:

$$\dot{R}_f = \frac{Re_l}{4} \left[(P_{gas} - P_l) R_f - \frac{2}{We} \right] \tag{18}$$

The initial conditions of the second problem stem from the state of the microbubble at the time of the rupture. Consequently, the initial microbubble shell radius for the second part of the problem is the one that the microbubble had when it broke. The same holds for the shell's expansion velocity and the pressure of the surrounding liquid. The pressure of the gas for the moment right after the rupture has changed and it is calculated through $Eq. 18$ using the data from the parametric analysis.
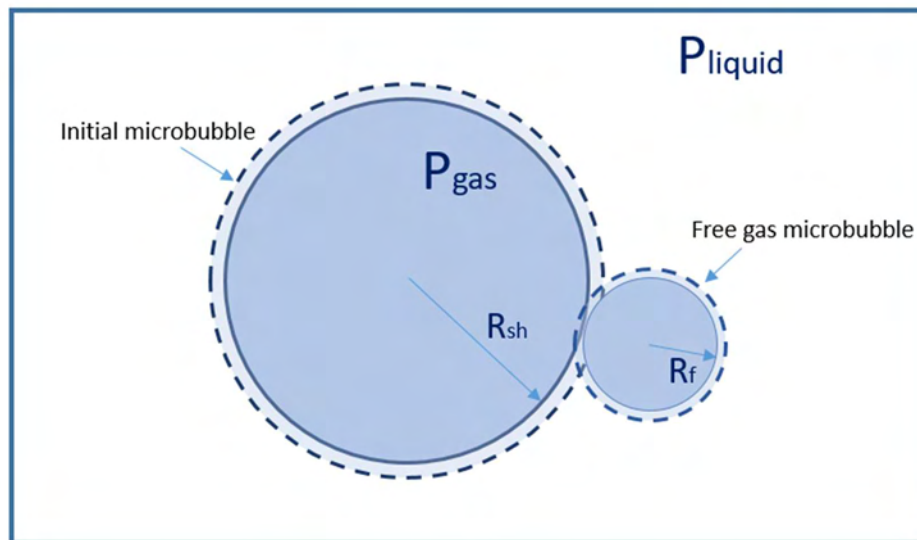
The broken microbubble problem

Figure 5 Depiction of the oscillating microbubble shell and attached free gas microbubble

The second part begins at a chosen time right after the microbubble is ruptured, according to the data provided by Bouakaz et al., and the encapsulated gas is released [30]. That time is considered to be right before the point of maximum expansion of the microbubble after a few cycles of undisturbed pulsation. The same acoustic signal continues to be applied onto a system, comprising of the microbubble and a free gas bubble created by the leaked gas that continues to oscillate, as it is plainly depicted in *Fig.5*. The two microbubbles oscillate separately, but they mutually affect each other through the shared internal gas pressure.

Assumptions

The assumptions that were made for the intact microbubble problem are valid through the second part of the problem where the microbubble is broken and a new free gas bubble has emerged. A few more assumptions are needed for the simulation of the system pulsations:

- Rupture occurs right before the maximum expansion of the microbubble after three cycles of oscillations, according to the optical observations performed on a PB-127 microbubble by Bouakaz et al.
- Spherosymmetric pulsations are assumed for the free microbubble as well as the broken microbubble shell.
- The emerging microbubble is considered to be attached on the matrix microbubble while they oscillate.
- The oscillation of the microbubble shell and the emerging free microbubble are simulated as two separate procedures.
- The pressure of the gas inside the two microbubbles is the same.
- The free gas microbubble does not have a coating.
- The shear stress modulus (G) and the dynamic viscosity (μ) are taken equal to zero for the part of the simulation referring to the free gas microbubble.

Initial conditions

All the initial conditions of the intact microbubble problem are valid throughout the broken microbubble problem as well.

The additional initial conditions that were necessary for the second part of the problem are a result of the transitional parametric analysis.

The microbubble shell radius and its velocity are considered to be the same as the ones at the point of rupture which are $R_{sh} = 2.09104\ \mu m$ and $\dot{R}_{sh} = 0.19046\ \mu m/\mu s$.

The initial radius of the free gas microbubble assumes the value $R_f = 0.176\ \mu m$, which is approximately one tenth of the initial value for the microbubble shell radius for the second part of the problem. The free gas microbubble radius is, according to the results of the parametric analysis, $\dot{R}_f = 0.346521939\ \mu m/\mu s$.

The initial gas pressure is $P_{gas} = 0.087492\ MPa$ right after the point of rupture, as calculated by $Eq.\ 17$. The pressure difference on the surface of the microbubble shell is $\Delta P = P_{gas} - P_{liquid} = 0.80770$ MPa.

Governing equations

The microbubble is linked to the free bubble formed through the internal pressure of the gas. Since an extra radius referring to the free gas microbubble is inserted, the governing equations of the intact problem, which still stand, are transformed accordingly and take the following form. The pressure of the surrounding liquid on the surface of the free gas microbubble is:

$$P_{l_{r=R_f}} = \left[\frac{2}{We} + P_{stat}\right]\left(\frac{1}{R^3 + R_f^3}\right)^{\gamma} - \frac{2}{WeR_f} - \frac{4}{Re_l}\frac{\dot{R}_f}{R_f} \qquad [19]$$

And the equation describing its spherosymmetric oscillations is:

$$\left(1 - M\dot{R}_f\right)R_f\ddot{R}_f + \left(\frac{3}{2} - \frac{M\dot{R}_f}{2}\right)\dot{R}_f^2 = \left(1 + M\dot{R}_f\right)\left(P_{l_{r=R}} - P_{st} - P_{AC}\right) + MR_f\frac{d}{dt}\left(P_{l_{r=R}} - P_{AC}\right) \qquad [20]$$

The scattered pressure signal of the pulsating microbubble shell and the free gas microbubble combined is a result of the addition of the individual scattered signals. $Eq.\ 5$ is applied for both the microbubble shell and the free gas microbubble in the same manner. [35]

$$P_{scattered} = \frac{R_{sh}^2}{dist}\ddot{R}_{Sh} + \frac{2R_{Sh}}{dist}\dot{R}_{Sh}^2 - \left(\frac{R_{Sh}}{dist}\right)^4\frac{\dot{R}_{sh}^2}{2} + \frac{R_f}{dist}\left(R_f\ddot{R}_f + 2\dot{R}_f^2\right) - \left(\frac{R_f}{dist}\right)^4\frac{\dot{R}_f^2}{2} \qquad [21]$$

The scattering cross section and the RMS scattered pressure are calculated in the same way as in $Eq.\ 8$ and 9, using the $P_{scattered}$ found in $Eq.\ 21$

3. Numerical Analysis

The solution of both parts of the problem involves a 2nd order nonlinear Ordinary Differential Equation (ODE). These are $Eq.\,3$ and $Eq.\,20$ respectively for the intact microbubble problem and the broken microbubble problem when $P_{l_{r=R}}$ is inserted via $Eq.\,4$ and $Eq.\,19$ respectively. The unknown values in these cases are the radii of the microbubbles, as well as the radii velocities as functions of time, while the only independent variable was time. For the numerical solution of these equations, a 4th order Runge-Kutta iterative method was employed for each of the unknown variables. The iterative method used the initial values that were provided for the problems in order to produce the value of the unknown variables for the next timestep. An indicative example of the way the iterative method was employed is shown below:

$$K_1(1) = dt * \dot{R}(t)$$
$$K_1(2) = dt * \ddot{R}(t)$$
$$K_2(1) = dt * \dot{R}\left(t + \frac{dt}{2}\right)$$
$$K_2(2) = dt * \ddot{R}\left(t + \frac{dt}{2}\right)$$
$$K_3(1) = dt * \dot{R}\left(t + \frac{dt}{2}\right)$$
$$K_3(2) = dt * \ddot{R}\left(t + \frac{dt}{2}\right)$$
$$K_4(1) = dt * \dot{R}(t + dt)$$
$$K_4(2) = dt * \ddot{R}(t + dt)$$

$$R(t+1) = R(t) + dt/6 * (K_1(1) + 2 * K_2(1) + 2 * K_3(1) + K_4(1))$$
$$\dot{R}(t+1) = \dot{R}(t) + dt/6 * (K_1(2) + 2 * K_2(2) + 2 * K_3(2) + K_4(2))$$

The numbered subscripts refer to the steps of the iterative method, while the numbers in the parentheses of every K variable refer to the solution of the radius (1) or velocity (2) of the problem being solved at the time. Variable dt refers to the timestep used for the numerical method.

In the process of the Runge-Kutta method, it was necessary to find the value of the 2nd derivative of the respective radius for each timestep (acceleration of the shell/gas-liquid interface). That was achieved through the employment of functions, such as $D2RDTF2$ that managed the solution of $Eq.\,3$ and $Eq.\,4$ for the part of the microbubble shell oscillation alone.

During the simulation of the problem, there were some times when instabilities presented in the results or prevented the simulation from continuing due to infinitesimal or negative values. That problem was addressed with the decrease of the timestep, which allowed for more accurate results. An adequate timestep value was found to be $10^{-5}\mu s$.

When the existence of the free gas microbubble was introduced, in the second part of the problem, the need for an additional part to the code that handled the new equations properly, emerged.

It was observed that the free gas bubble expands along with the original microbubble with a small phase difference. When the polymer shelled microbubble contracts, though, the gas bubble completely disappears inside the matrix bubble. That, numerically, translates to extremely small or negative values for the radius of the free gas bubble and causes the free bubble's expansion velocity to acquire very high values that cannot be physically explained.

This happens because the forces that keep the free gas microbubble connected to the shell are not taken into account during the simulation. In order to overcome this difficulty, the addition of a "switch" that ensured the radius of the gas bubble would only acquire positive values was needed. Particularly, when the microbubble value is lower than one tenth of the initially given one, the simulation changes to solving only for the microbubble shell pulsations, immediately assigns the initial value to the free gas microbubble radius and its velocity, and changes back to solving for both the microbubbles in the next timestep.

Realistically, it would be desired for the radius of the gas bubble to have negative values during the time when the gas bubble is entirely inside the shell in order to describe the problem accurately. That was impossible, though, in the way the problem was formulated in this study.

4. Results and discussion

The results that occurred by running the simulation of the problem described in *Problem Formulation* with the initial values that came out of the short parametric study that took place, are illustrated in the following diagrams.

The intact microbubble problem

Assuming that the circumstances had failed to rupture the microbubble, the pulsation of the intact polymer coated microbubble would be the one described in *Fig.6*. The point in time at which the rupture occurs under the current circumstances is marked by the red dashed line. It is, as previously stated, right before the maximum point of expansion of the microbubble.

The microbubble pulsates normally and in agreement to the fluctuations of the pressure of the encapsulated gas. The gas pressure rises when the microbubble shell contracts and decreases during expansion, as shown in *Fig.7*. For an elastic shell the in plane stresses are maximized during expansion as a result of which the shell may be torn apart, which is what apparently happens in the experimental study carried out by Bouakaz et al. [30]. Regarding the moment of fracture, it can be observed that both the pressure of the surrounding liquid and the pressure of the encapsulated gas are at their lowest points resulting to a very high pressure difference being imposed on the shell of the microbubble as seen in *Fig. 8*.
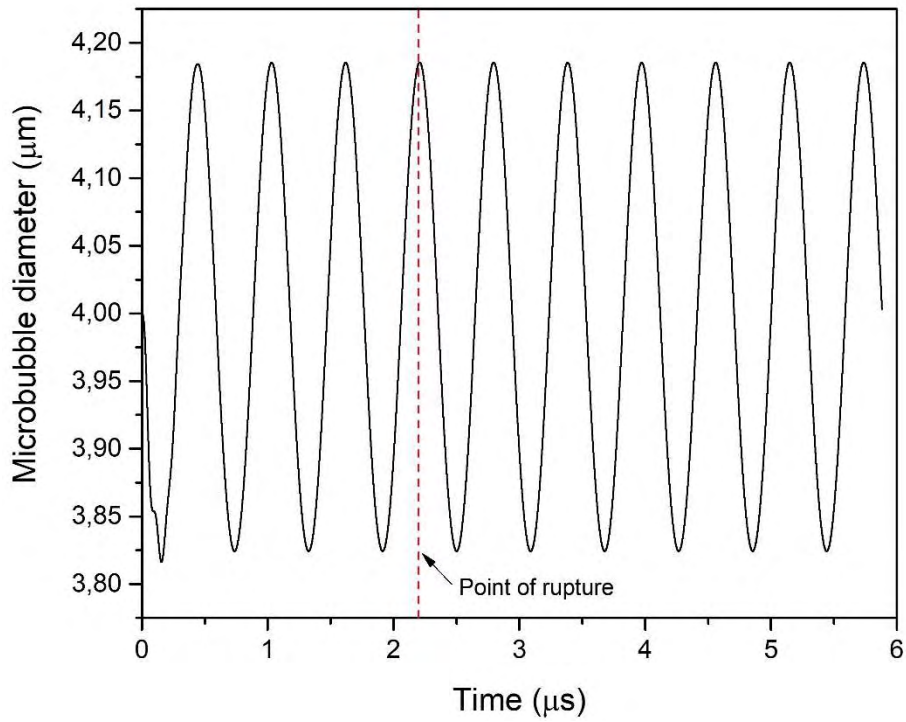
Figure 6 Pulsation of the intact microbubble with a 4µm diameter under an acoustic signal of 10 cycles and 1.7MHz
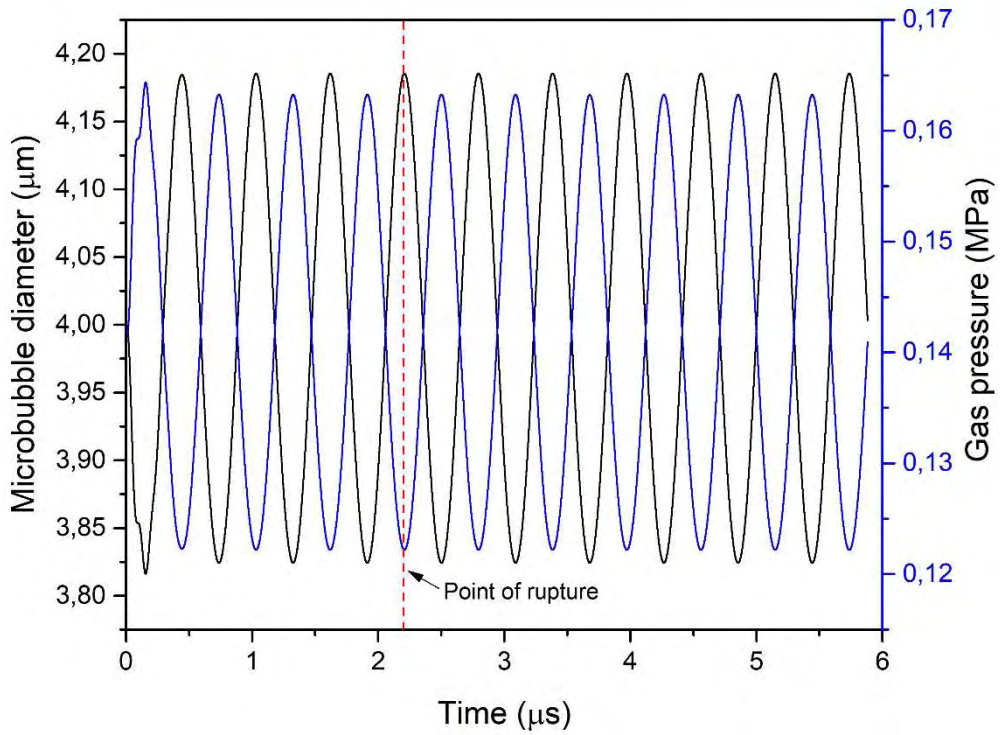

Figure 7 Pulsations of the microbubble in relation to the pressure of the encapsulated gas
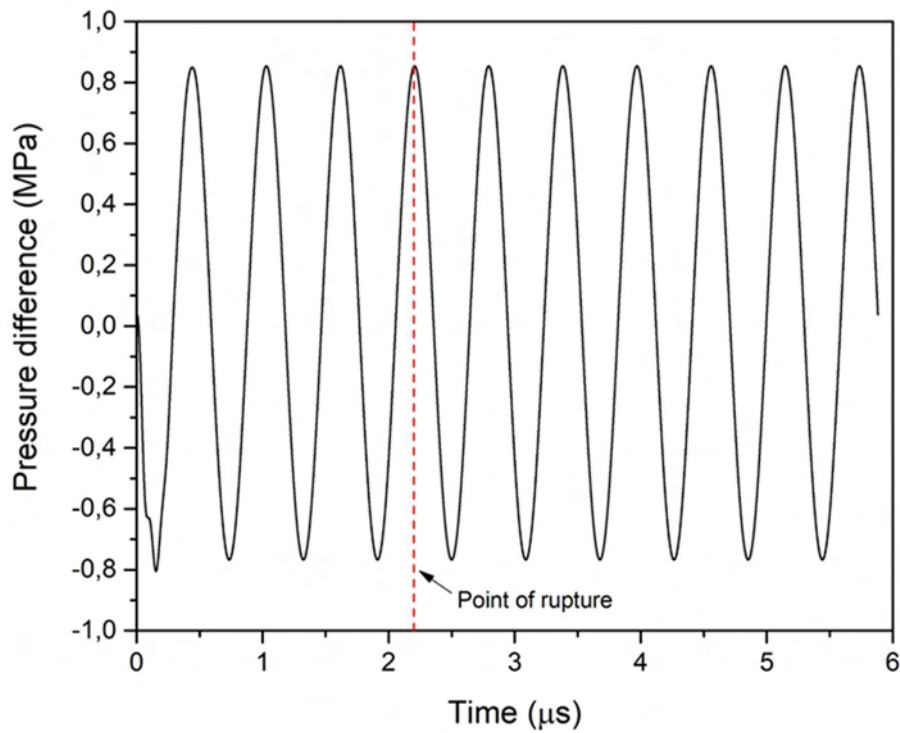
Figure 8 The pressure difference between the encapsulated gas and the surrounding liquid during the intact problem pulsations

The total scattering cross section of the scattered pressure signal is calculated through $Eq.8$ for the intact microbubble problem and it is $SCS = 0,02436\ \mu m^2$. The respective SCSs for different harmonics are listed in *Table II.*

Table II Scattering cross section in relation to harmonics

	Scattering cross section (μm^2)
Subharmonic	0,000018
1st Harmonic	0,01627817
2nd Harmonic	0,000170965
3rd Harmonic	0,00002934

It can be observed that the sum of the harmonics' scattering cross sections is roughly, but not exactly, the same as the total. This is due to the existence of more than the presented harmonics because of the relatively wide amplitude of the pulsations. The SCS of the 1st harmonic though is the most influencing one. The RMS scattered pressure is calculated to be $P_{sc,RMS} = 18041,406\ Pa$, as found by $Eq.9$. The respective RMS scattered pressures for different harmonics are listed in *Table III*.

Table III RMS scattered pressure in relation to harmonics

	$P_{sc,RMS}\ (Pa)$
Subharmonic	478,7254
1st Harmonic	14548,395
2nd Harmonic	1165,9152
3rd Harmonic	609,78089

Transition to the broken microbubble problem

The parametric study that involves the equations described in *Problem formulation: Transition to the broken microbubble problem* examined as potential moments of rupture the ones that came shortly before the maximum expansion of the microbubble shell, after a few cycles of oscillation. An indicative part of the results is presented in *Table IV.* It is obvious that there is minimal difference between the results when it comes to the value of the free microbubble radius velocity between the times of rupture that are close to the maximum point of expansion. The choice was made through observation of the results that were produced by the available data, opting for a smooth transition from the previous oscillation pattern to the one occurring after rupture of the microbubble shell, while considering the information coming from the optical observations made by Bouakaz et al. [30]. Significant part in the final decision played the value of the gas-liquid interface velocity of the emerging microbubble $(\dot{R}_f)$, which was required to be positive but relatively low, in order for the free gas microbubble to reach the experimentally observed oscillation amplitude, while the value of the initial free microbubble radius was required to be close to one tenth of the initial microbubble shell radius.

Table IV Parametric analysis results

R_{sh} (μm)	P_{liquid} (MPa)	$\dot{R}_f(\frac{\mu m}{\mu s})$			
		$R_{f0} = 0.17\mu m$	$R_{f0} = 0.176\mu m$	$R_{f0} = 0.18\mu m$	$R_{f0} = 0.20\mu m$
2,0924	-0.730517	-1,24195	-0,01544	0,802216	4,890246
2,09241	-0.730568	-1,23984	-0,01325	0,804456	4,892736
2,09242	-0.730619	-1,23776	-0,0111	0,806659	4,895183
2,09242	-0.730668	-1,23566	-0,00892	0,808884	4,897656
2,09243	-0.730717	-1,23365	-0,00684	0,811012	4,90002
2,09244	-0.730765	-1,23167	-0,0048	0,813101	4,902341
2,09245	-0.730812	-1,22974	-0,00279	0,815152	4,904621
2,09245	-0.730858	-1,22778	-0,00076	0,817226	4,906925
2,09246	-0.730903	-1,22591	0,001168	0,819202	4,909121
2,09247	-0.730947	-1,22408	0,003063	0,821141	4,911274
2,09247	-0.730991	-1,22223	0,00498	0,823101	4,913453
2,09248	-0.731034	-1,22047	0,006802	0,824964	4,915522
2,09249	-0.731075	-1,21875	0,008586	0,826788	4,917549
2,09249	-0.731116	-1,217	0,010392	0,828635	4,919602
2,0925	-0.731157	-1,21535	0,012102	0,830384	4,921545
2,09251	-0.731196	-1,21373	0,013775	0,832095	4,923446
2,09251	-0.731235	-1,2121	0,01547	0,833829	4,925372
2,09252	-0.731272	-1,21055	0,017069	0,835464	4,92719
2,09253	-0.731309	-1,20904	0,018631	0,837062	4,928965
2,09253	-0.731345	-1,20751	0,020215	0,838682	4,930765

The final choice for the moment of rupture is displayed in *Table V*.

R_{f0} (μm)	R_{sh} (μm)	P_{liquid} (MPa)	$\dot{R}_f(\dfrac{\mu m}{\mu s})$
0,18	2,09104	-0,720208	0,346521939

The broken microbubble problem

Fig.9 describes the way the diameter of the initial polymer shelled microbubble changed through time from the beginning of the simulation of the intact problem until the end of the broken microbubble problem. The first part of the simulation refers to the first approximately 2.2 μs, while the rest refers to the simulation of the second problem. It is obvious that the pulsations of the microbubble shell remain almost the same before and after the rupture. The pulsation of the microbubble shell is only slightly affected by the pulsation of the free gas microbubble when it is at its maximum point of contraction. At this time, the free gas microbubble is, in reality, inside the polymer shell. Since the simulation does not cover this part correctly, the values of the microbubble shell diameter are altered.
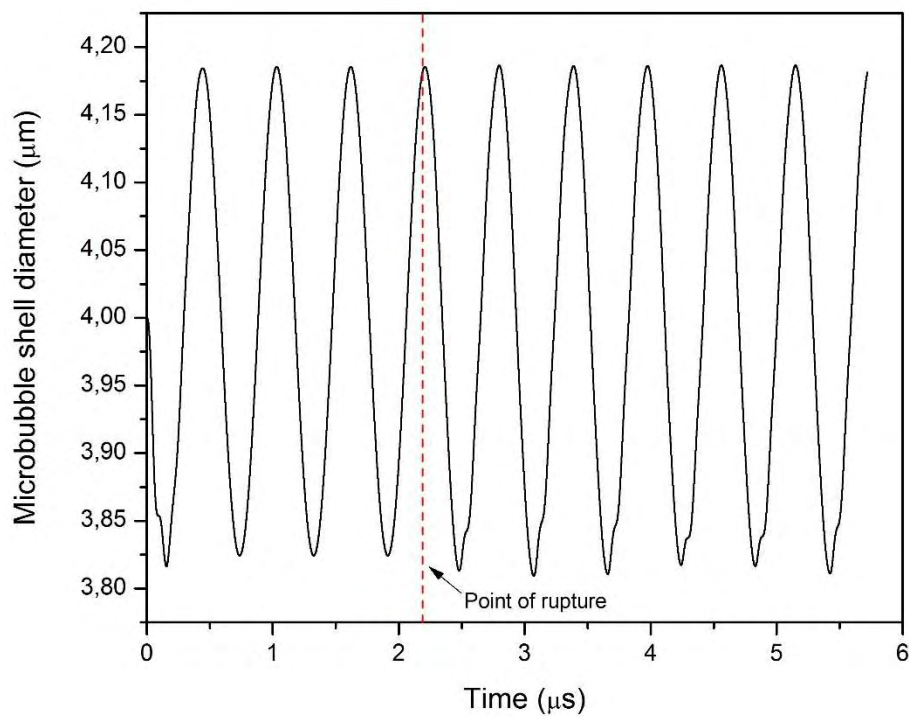

Figure 9 Pulsation of the microbubble shell before and after it brakes

Fig.10 presents the pulsations of the shell and free microbubble diameters in time. The amplitude of the free microbubble oscillations is not stabilized during the insonification period.
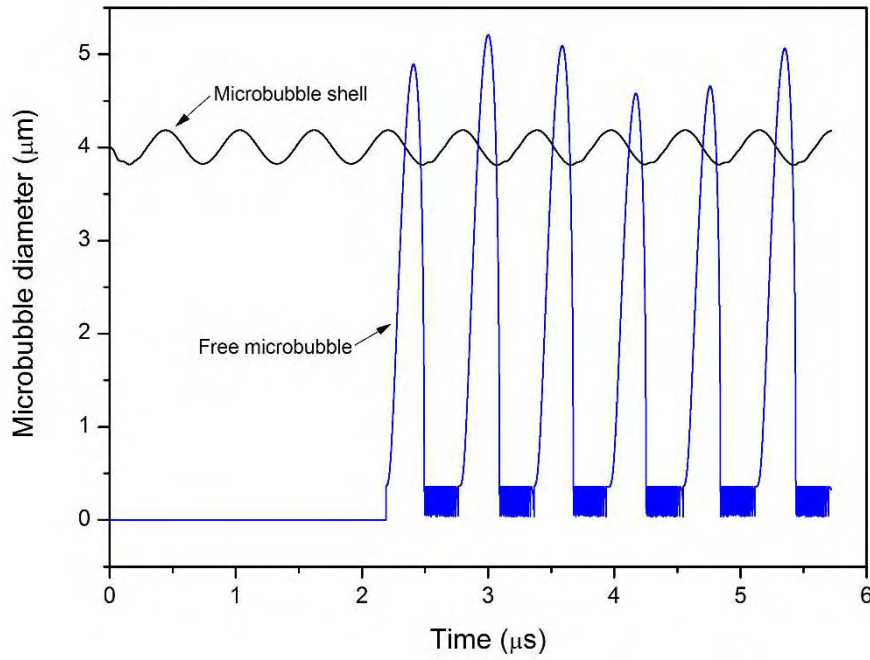
Figure 10 The pulsation of the microbubble shell and the occurring free microbubble through the simulation time of both problems
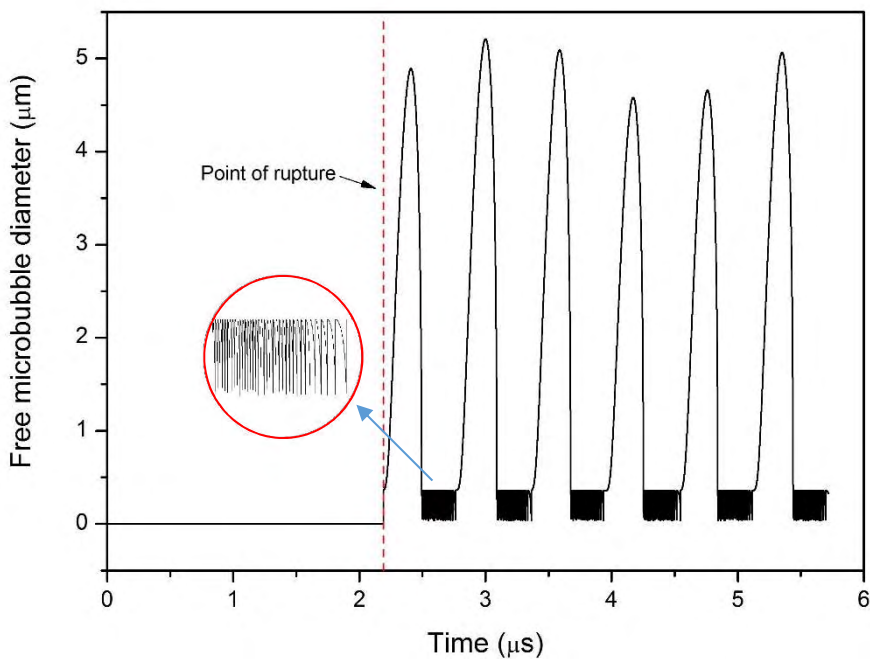
Figure 11 The pulsation of the free microbubble through time

The rapid oscillations that appear for the lower values of the free microbubble diameter (*Fig.11*) are related to the pressure of the surrounding liquid as shown in *Fig.15*. In more detail, what happens is that when the free microbubble enters the shell after a pulsation, it is given the initial values of radius and velocity that were chosen. In the next timestep the free microbubble is attempting to start oscillating again with the imposed amplitude, but the pressure conditions are not allowing this movement. Therefore, the free microbubble oscillates with a smaller allowed amplitude until the liquid pressure reaches its lowest value.

This is easier to observe in *Fig. 15* where the movement of the free gas microbubble is presented in relation to the pressure of the surrounding liquid.

During the optical observations of the pulsating microbubbles, they are addressed as one entity and their oscillations are portrayed as one diameter-time diagram. [30] This way of presentation is depicted in *Fig.12*. The sum of the individual diameters is referred to as effective diameter.
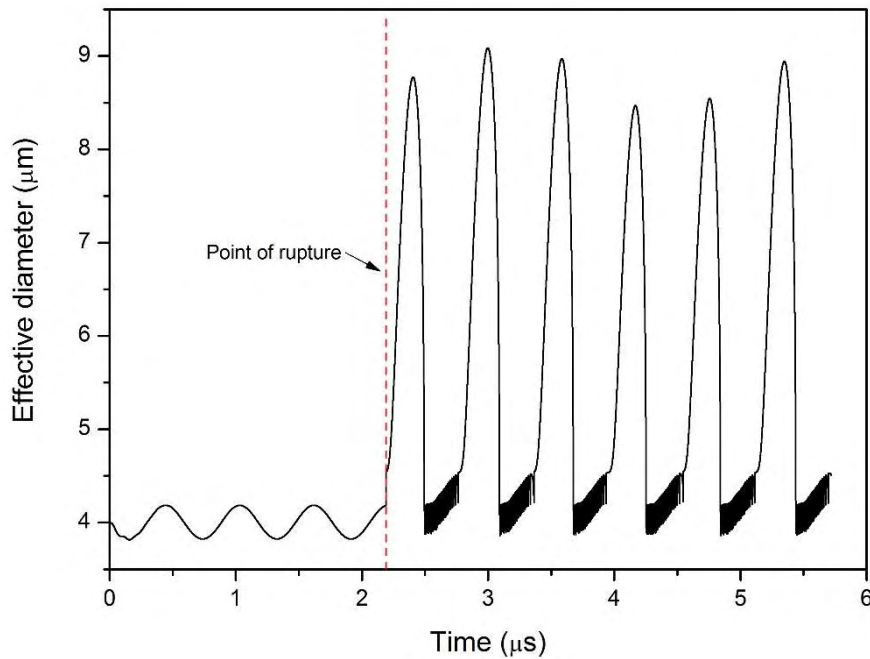

Figure 12 Effective diameter oscillations of a 4µm initial microbubble and the occurring attached free microbubble
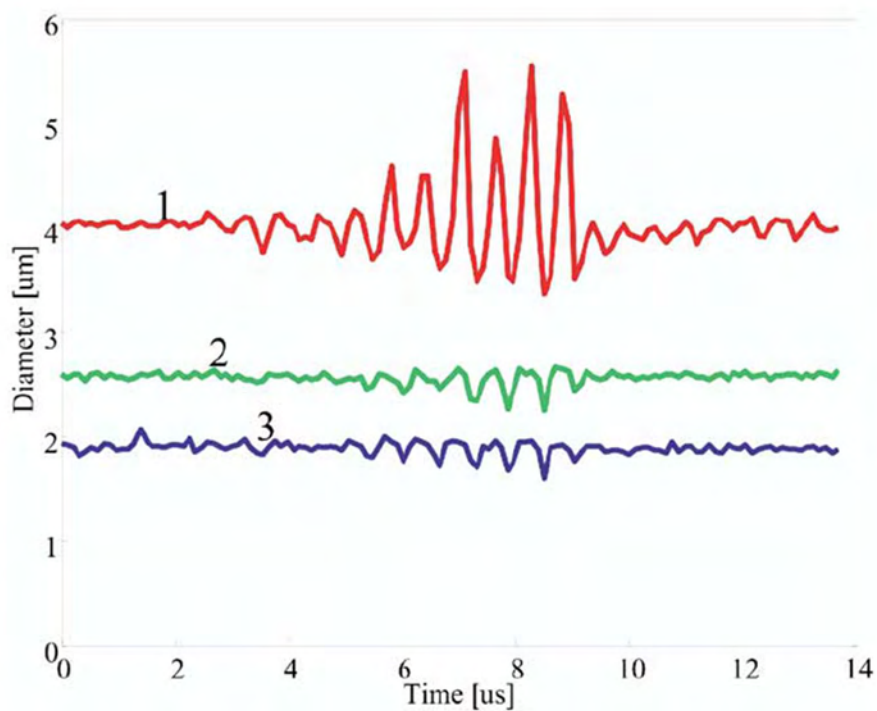

Figure 13 Effective diameter oscillations as observed by Bouakaz et.al *[30]*

32

The effective diameter of the microbubble shell and the free gas bubble takes higher values than it did during the intact part of the problem because the diameter of the gas bubble is added. The deviation from the experimental observations is due to the fact that the forces connecting the free gas microbubble to the shell and preventing it from detaching were neglected.

Following the behavior of the 4μm diameter microbubble in *Fig.13*, it can be observed that there is a period of undisturbed oscillation in the beginning, a transitional period of a little more than one cycle and then a period of higher amplitude oscillations that involve the free gas microbubble that has emerged before it dissolves. A similar pattern can be seen in *Fig. 12* in regard to the three distinct periods of oscillation.

The pressure of the encapsulated gas is affected by the free microbubble pulsations in the way portrayed in *Fig.14.* The added volume that the expansion of the free microbubble offers in addition to the already expanded microbubble shell leads to a measurable drop in the gas pressure.
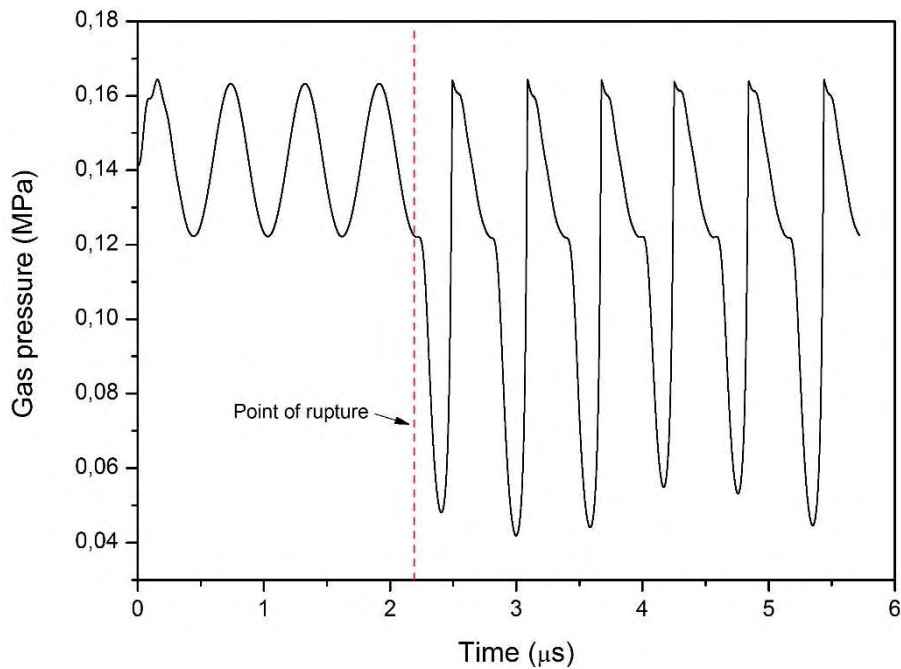

Figure 14 Pressure of the encapsulated gas before and after the rupture of the microbubble shell

The behavior of the free gas microbubble is related to the pressure of the surrounding liquid in the way shown in *Fig. 15*. When the liquid pressure reaches its lowest points the free microbubble is able to expand again and get out of the small amplitude pulsation loop it was in.
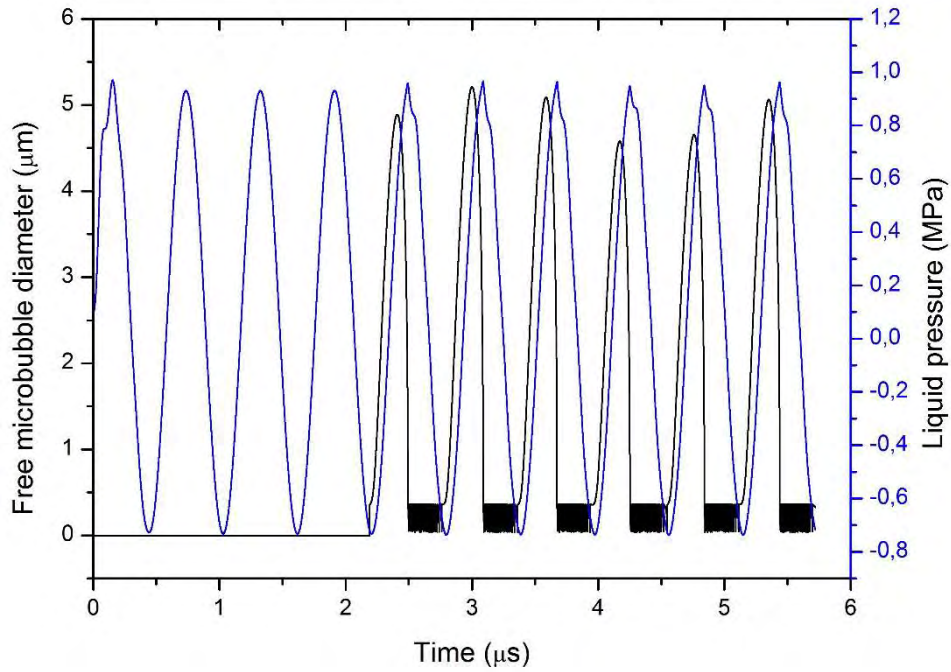
Figure 15 Free gas microbubble diameter representation in relation to the pressure of the surrounding liquid

The total scattering cross section that has been calculated for the second part of the problem, where both microbubbles pulsate is $SCS = 298,68955 \ \mu m^2$, which is a much higher value than the one calculated for the intact problem. This can be justified by the existence of an uncoated microbubble in the pulsating system. The respective SCSs for different harmonics are listed in *Table VI.*

Table VI Scattering cross section in relation to harmonics for two pulsating microbubbles

	Scattering cross section (μm^2)
Subharmonic	0,0000231882
1st Harmonic	0,39042
2nd Harmonic	3,01507
3rd Harmonic	3,59131

The sum of all the existing harmonics of the problem was calculated to be $SCS = 297,48792 \ \mu m^2$ which is higher than the SCS sum of the first 3 harmonics and indicates the existence of more than the presented harmonics in the problem. The RMS scattered pressure is calculated to be $P_{sc,RMS} = 52,5866 \ Pa$, which is a much lower value than the one calculated for the intact problem, and the same holds for the RMS scattered pressures for the different harmonics of the insonification listed in *Table VII*.

Table VII RMS scattered pressure in relation to harmonics for two pulsating microbubbles

	$P_{sc,RMS}$ (Pa)
Subharmonic	0,01468
1st Harmonic	1,90505
2nd Harmonic	5,29406
3rd Harmonic	5,77786

Comparing the results concerning the scattering cross section and the RMS scattered pressure of the two parts of the problem it is noticeable that the SCS total value is a lot higher in the broken microbubble problem than in the intact one. It can also be observed that the broken microbubble free gas bubble system produces a broadband SCS spectrum, since the sum of the values of the presented harmonics is not close to the total SCS value. On the other hand, the RMS scattered pressure was a lot lower for the broken microbubble problem.

5. Conclusions

The main objective of this thesis was to evaluate if the behavior of a coated microbubble in a liquid environment under the influence of an acoustic signal could be simulated using the proposed mathematical model. The model was based on the Kelvin-Voigt constitutive law for small displacements of a membrane-like material.

The part of the problem where the microbubble remained intact was simulated successfully and the results that were produced resembled those of the experimental observations made by Bouakaz et al. on the same subject [30]. The point of rupture was chosen after a parametric analysis based on the expansion velocity of the emerging microbubble. The rupture occurred at a point where the pressure difference between the encapsulated gas and the surrounding liquid on the surface of the microbubble was very high. During the second part of the problem, the microbubble shell and free gas microbubble oscillations were simulated as two different procedures. The pulsations of the effective diameter of the microbubble shell and free gas microbubble resembled those of the experimentally observed system. The pulsations of the free microbubble though added a wider amplitude to the sum because the inertia forces keeping the free microbubble connected to the shell were not taken into account. During the simulations, it was possible to document the scattering cross section for each case, as well as the root-mean-squared scattered pressure. These were found to be particularly different for each case and, thus, could serve as an identifier of the condition of the microbubble.

The deductions that were made from the results of the numerical simulation of the problem validate the initial assumption about the behavior of the microbubble to some extent. It was not possible, however, to simulate the pulsations of the microbubble shell and free gas bubble system accurately with the assistance of the methods described in Methodology, especially concerning the pulsation amplitude of the free microbubble and the part of the pulsation when the free microbubble is observed to retreat back into the shell.

To summarize, the results of the present thesis reveal that, while coated microbubbles can be a powerful tool in ultrasound imaging enhancement, the behavior of a broken microbubble pulsating in an aqueous environment under the circumstances investigated cannot be accurately simulated as a system of two independently pulsating microbubbles using the proposed mathematical model.

It remains to be validated if an encapsulated microbubble has the potential to be utilized as a contrast enhancement agent after the rupture of its shell. An in depth investigation of the backscatter signal of the broken microbubble is very likely to point towards this direction. Another important information that needs to be investigated further is the ability of a broken microbubble to be recognized by the backscatter signal it emits and its difference to the one emitted by an intact microbubble of the same type.

Further research on the subject would be especially useful. A proposed way in which the problem of the oscillating microbubble before and after the rupture of the shell could be approached is by the method of boundary elements on the microbubble shell and the free gas bubble treated as a compound particle. A simplified representation of the behavior of the microbubble and free gas bubble unity is portrayed in *Fig. 16*.
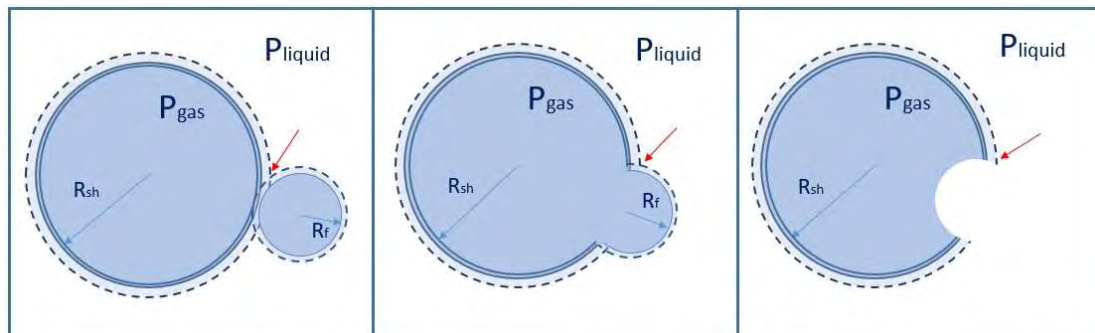

Figure 16 Presentation of the stages of the pulsating microbubble system

Particular attention should be given to the boundary conditions at the point where the microbubble shell and the outer surface of the free gas microbubble are joined (red arrows), as well as, the equilibrium equations on the surface of the initial microbubble and the free gas bubble.

Bibliography

[1] K. Efthymiou, "Interaction of microbubble with elastic casing (contrast agent) with adjacent wall in the presence of acoustic disorders," 2015.

[2] D. H. Thomas, M. B. Butler, V. Sboros, K. Efthymiou and N. Pelekasis, "The effect of resonance on transient microbubble response; experimental and theoretical observations.".

[3] S. R. Sirsi and M. A. Borden, "Microbubble compositions, properties and biomedical applications," *Bubble Science, Engineering & Technology,* vol. 1, no. 1-2, pp. 3-17, 2009.

[4] C. Christiansen, H. Kryvi, P. Sontum and T. Skotland, "Physical and biochemical characterization of Albunex, a new ultrasound contrast agent consisting of air???filled albumin microspheres suspended in a solution of human albumin," *Biotechnology and Applied Biochemistry,* vol. 19, no. 3, pp. 307-320, 1994.

[5] S. Singhal, C. C. Moser and M. A. Wheatley, "Surfactant-Stabilized Microbubbles as Ultrasound Contrast Agents: Stability Study of Span 60 and Tween 80 Mixtures Using a Langmuir Trough," *Langmuir,* vol. 9, no. 9, pp. 2426-2429, 1993.

[6] E. Dressaire, R. Bee, D. C. Bell, A. Lips and H. A. Stone, "Interfacial polygonal nanopatterning of stable microbubbles," *Science,* vol. 320, no. 5880, pp. 1198-1201, 2008.

[7] J. S. D'Arrigo, Stable Gas-in-Liquid Emulsions - Production in Natural Waters and Artificial Media, vol. 19, 2003, pp. 317-323.

[8] R. Notter and Z. Wang, "Pulmonary surfactant: Physical chemistry, physiology and replacement," *Reviews in Chemical Engineering, 13(4),* 1997.

[9] R. E. Pattle, *Properties, function and origin of the alveolar lining layer [7],* vol. 175, 1955, pp. 1125-1126.

[10] D. H. Kim, M. J. Costello, P. B. Duncan and D. Needham, "Mechanical properties and microstructure of polycrystalline phospholipid monolayer shells: Novel solid microparticles," *Langmuir,* vol. 19, no. 20, pp. 8455-8466, 2003.

[11] S. H. Bloch, M. Wan, P. A. Dayton and K. W. Ferrara, "Optical observation of lipid- and polymer-shelled ultrasound microbubble contrast agents," *Applied Physics Letters,* vol. 84, no. 4, pp. 631-633, 2004.

[12] S. Qin, C. F. Caskey and K. W. Ferrara, "Ultrasound contrast microbubbles in imaging and therapy: Physical principles and engineering," *Physics in Medicine and Biology,* vol. 54, no. 6, 2009.

[13] M. Postema and G. Schmitz, *Bubble dynamics involved in ultrasonic imaging,* vol. 6, 2006, pp. 493-502.

[14] J. E. Chomas, P. Dayton, D. May and K. Ferrara, "Threshold of fragmentation for ultrasonic contrast agents," *Journal of Biomedical Optics,* vol. 6, no. 2, p. 141, 2001.

[15] K. Morgan, P. Dayton, A. Klibanov, G. Brandenburger, K. Nightingale and K. Ferrara, *IEEE Transactions on Ultrasonics Ferroelectrics and Frequency Control.,* p. 44:1264–1277, 1997.

[16] T. G. Leighton, "The Acoustic Bubble," *The Journal of the Acoustical Society of America,* vol. 96, p. 2616, 1994.

[17] L. Hoff, Acoustic Characterization of Contrast Agents for Medical Ultrasound Imaging, Boston: Kluwer Academic Publishers, 2001.

[18] V. Sboros, *Response of contrast agents to ultrasound,* vol. 60, 2008, pp. 1117-1136.

[19] S. Mehier-Humbert, F. Yan, P. Frinking, M. Schneider, R. H. Guy and T. Bettinger, "Ultrasound-mediated gene delivery: Influence of contrast agent on transfection," *Bioconjugate Chemistry,* vol. 18, no. 3, pp. 652-662, 2007.

[20] R. Gramiak and P. Shah, "Echocardiography of the Aortic Root. : Investigative Radiology," *Investigative Radiology,* vol. 3, no. 5, pp. 356-366, 1968.

[21] V. Paefgen, D. Doleschel and F. Kiessling, *Evolution of contrast agents for ultrasound imaging and ultrasound-mediated drug delivery,* vol. 6, 2015.

[22] "Collins Dictionary," [Online]. Available: www.collinsdictionary.com/submission/11018/Theranostics.

[23] S. B. Feinstein, J. Cheirif, F. J. Ten Cate, P. R. Silverman, P. A. Heidenreich, C. Dick, R. M. Desir, W. F. Armstrong, M. A. Quinones and P. M. Shah, "Safety and efficacy of a new transpulmonary ultrasound contrast agent: Initial multicenter clinical results," *Journal of the American College of Cardiology,* vol. 16, no. 2, pp. 316-324, 1990.

[24] K. Bjerknes, J. Braenden, J. Braenden, R. Skurtveit, G. Smistad and I. Agerkvist, *Journal Of Microencapsulation,* p. 18:159–171, 2001.

[25] P. Narayan and M. Wheatley, "Preparation and characterization of hollow microcapsules for use as ultrasound contrast agents," *Polymer Engineering and Science,* pp. 2242 - 2255, 1999.

[26] W. J. Cui, J. Z. Bei, S. G. Wang, G. Zhi, Y. Y. Zhao, X. S. Zhou, H. W. Zhang and Y. Xu, *Journal of Biomedical Materials Research Part B-Applied Biomaterials.,* p. 73B:171–178., 2005.

[27] F. Cavalieri, A. El Hamassi, E. Chiessi and G. Paradossi, "Stable polymeric microballoons as multifunctional device for biomedical uses: synthesis and characterization.," *Langmuir,* pp. 8758-8764, 2005.

[28] M. R. Bohmer, R. Schroeders, J. M. Steenbakkeres, S. de WInter, P. A. Duineveld, J. Lub, W. M. Nijssen, J. A. Pikkemaat and H. R. Stapert, *Colloid Surf A-Physicochem Eng Asp.,* p. 289:96–104, 2006.

[29] A. P. Patrianakos and M. I. Hamilos, "PB-127, a novel contrast agent for the detection of myocardial perfusion," *Current Opinion in Investigational Drugs,* vol. 8, no. 3, pp. 248-255, 2007.

[30] A. Bouakaz, M. Versluis and N. De Jong, "High-speed optical observations of contrast agent destruction," *Ultrasound in Medicine and Biology,* pp. 391-399, 2005.

[31] N. de Jong, "Technical note: Mechanical Index," *Eur J Echocardiography,* vol. 3, pp. 73-74, 2002.

[32] A. Eller and H. G. Flynn, "Rectified diffusion during nonlinear pulsations of cavitation bubbles," *J. Acoustic Society of America,* vol. 37, pp. 493-503, 1965.

[33] M. M. Fyrillas and A. J. Szeri, "Dissolution or growth of soluble spherical oscillating bubbles," *Cambridge University Press,* pp. 381-407, 1994.

[34] L. Hoff, P. C. Sontum and J. M. Hovem, "Oscillations of polymeric microbubbles: Effect of the encapsulating shell," *The Journal of the Acoustical Society of America,* vol. 107, no. 4, pp. 2272-2280, 2000.

[35] K. Tsiglifis and N. A. Pelekasis, "Nonlinear radial oscillations of encapsulated microbubbles subject to ultrasound: The effect of membrane constitutive law," *The Journal of the Acoustical Society of America,* vol. 123, no. 6, pp. 4059-4070, 2008.

[36] K. Vokurka, "On Rayleigh's model of a freely oscillating bubble. I. Basic relations," *Czechoslovak Journal of Physics,* vol. 35, no. 1, pp. 28-40, 1985.

[37] A. Lytra, "Numerical & theoretical study of the static response of coated microbubbles subject to uniform and distributed load-application on the estimation of the shell elastic properties," 2017.

Appendix A

The equations needed for the parametric analysis in the transitional part of the problem were solved in a Matlab computational environment. The code written for this reason is attached here.

```
R0=2*10^(-6);

rhol=998.0;

mu=10^(-3);

Pinf=1.01*10^5;

sigma=0.072;

omega=2*3.141592653589*1.7*10^(6);

Rb=0.176*10^(-6);

gama=1.07;


Rsh=importdata('Rsh.txt');

Rsha=Rsh.*10^(-6);

Pl=importdata('Pl.txt');


We=rhol.*(R0^3)*(omega.^2)/sigma;

Rel=rhol.*omega.*(R0.^2)/mu;

Pstat=Pinf./(rhol.*(R0^2)*(omega.^2));

Pld=Pl./(rhol*(R0^2)*(omega^2));

Rshd=Rsha./R0;

Rbd=Rb./R0;


a=((Rbd.^3)+(Rshd.^3));

aa=1./a;

Pg=Pstat.*(aa.^gama);

Dpres=Pg-Pld;

Dpres1=dpres*(rhol*(R0^2)*(omega^2));

b=Pstat.*(aa.^gama)-Pld;

Rbdotd=(Rel./4)*(Rbd.*b-(2/We));

 Rbdot=Rbdotd.*omega.*R0;
```

Appendix B

The part of the FORTRAN code that simulates the solution of the Runge-Kutta iterative method for both the intact and the broken microbubble problem, as well as, the pressure related switch that was used.

```fortran
do i=1,NUMSTEP

K1=0.0D0
K2=0.0D0
K3=0.0D0
K4=0.0D0

Kf1=0.0D0
Kf2=0.0D0
Kf3=0.0D0
Kf4=0.0D0

RRADIUS=R
RDRDT=DRDT

RRADIUSf=Rf
RDRDTf=DRDTf


if (Rf.ge.Rf0/10.0) then

        iflug=1
        RRADIUS_prev=RRADIUS
        RDRDT_prev=RDRDT
        K1(1)=RDRDT
        K1(2)=D2RDTF(TIME,RRADIUS,RDRDT,RRADIUSf,RDRDTf)
        RRADIUS=R+0.5D0*TSTEP*K1(1)
        RDRDT=DRDT+0.5D0*TSTEP*K1(2)

        Kf1(1)=RDRDTf
        Kf1(2)=D2RDTFf(TIME,RRADIUSf,RDRDTf,RRADIUS_prev,RDRDT_prev)
        RRADIUSf=Rf+0.5D0*TSTEP*Kf1(1)
        RDRDTf=DRDTf+0.5D0*TSTEP*Kf1(2)

        RRADIUS_prev=RRADIUS
        RDRDT_prev=RDRDT
        K2(1)=RDRDT
        K2(2)=D2RDTF(TIME+0.5D0*TSTEP,RRADIUS,RDRDT,RRADIUSf,RDRDTf)
        RRADIUS=R+0.5D0*TSTEP*K2(1)
        RDRDT=DRDT+0.5D0*TSTEP*K2(2)

        Kf2(1)=RDRDTf
        Kf2(2)=D2RDTFf(TIME+0.5D0*TSTEP,RRADIUSf,RDRDTf,RRADIUS_prev,RDRDT_prev)
        RRADIUSf=Rf+0.5D0*TSTEP*Kf2(1)
        RDRDTf=DRDTf+0.5D0*TSTEP*Kf2(2)

        RRADIUS_prev=RRADIUS
        RDRDT_prev=RDRDT
        K3(1)=RDRDT
        K3(2)=D2RDTF(TIME+0.5D0*TSTEP,RRADIUS,RDRDT,RRADIUSf,RDRDTf)
        RRADIUS=R+TSTEP*K3(1)
        RDRDT=DRDT+TSTEP*K3(2)

        Kf3(1)=RDRDTf
        Kf3(2)=D2RDTFf(TIME+0.5D0*TSTEP,RRADIUSf,RDRDTf,RRADIUS_prev,RDRDT_prev)
        RRADIUSf=Rf+TSTEP*Kf3(1)
```

```fortran
      RDRDTf=DRDTf+TSTEP*Kf3(2)

      RRADIUS_prev=RRADIUS
      RDRDT_prev=RDRDT
      K4(1)=RDRDT
      K4(2)=D2RDTF(TIME+TSTEP,RRADIUS,RDRDT,RRADIUSf,RDRDTf)
      R=R+TSTEP/6.0D0*(K1(1)+2.0D0*K2(1)+2.0D0*K3(1)+K4(1))
      DRDT=DRDT+TSTEP/6.0D0*(K1(2)+2.0D0*K2(2)+2.0D0*K3(2)+K4(2))

      Kf4(1)=RDRDTf
      Kf4(2)=D2RDTFf(TIME+TSTEP,RRADIUSf,RDRDTf,RRADIUS_prev,RDRDT_prev)
      Rf=Rf+TSTEP/6.0D0*(Kf1(1)+2.0D0*Kf2(1)+2.0D0*Kf3(1)+Kf4(1))
      DRDTf=DRDTf+TSTEP/6.0D0*(Kf1(2)+2.0D0*Kf2(2)+2.0D0*Kf3(2)+Kf4(2))

else

      iflug=0
      RF=rf0 ; drdtf=drfdt
      K1(1)=RDRDT
      K1(2)=D2RDTF2(TIME,RRADIUS,RDRDT)
      RRADIUS=R+0.5D0*TSTEP*K1(1)
      RDRDT=DRDT+0.5D0*TSTEP*K1(2)

      K2(1)=RDRDT
      K2(2)=D2RDTF2(TIME+0.5D0*TSTEP,RRADIUS,RDRDT)
      RRADIUS=R+0.5D0*TSTEP*K2(1)
      RDRDT=DRDT+0.5D0*TSTEP*K2(2)

      K3(1)=RDRDT
      K3(2)=D2RDTF2(TIME+0.5D0*TSTEP,RRADIUS,RDRDT)
      RRADIUS=R+TSTEP*K3(1)
      RDRDT=DRDT+TSTEP*K3(2)

      K4(1)=RDRDT
      K4(2)=D2RDTF2(TIME+TSTEP,RRADIUS,RDRDT)
      R=R+TSTEP/6.0D0*(K1(1)+2.0D0*K2(1)+2.0D0*K3(1)+K4(1))
      DRDT=DRDT+TSTEP/6.0D0*(K1(2)+2.0D0*K2(2)+2.0D0*K3(2)+K4(2))

end if
```

The FORTRAN subroutine for the solution of Eq. 14 and Eq. 15 in order to obtain the value of $\ddot{R}_f$ following the pattern previously proposed by Dr. Eythymiou and Dr. Tsiglifis.

```fortran
REAL(8) FUNCTION D2RDTFf(TIME,Rf,DRDTf,R,DRDT)
IMPLICIT NONE
REAL(8) TIME,Rf,DRDTf,R,DRDT
REAL(8) OROS1,OROS2,OROS3,ARITH,PARON,ARITH1,ARITH2,EINFSEC
EINFSEC=EINF

OROS1=0.0D0
OROS2=0.0D0
ARITH=0.0D0
PARON=0.0D0
ARITH1=0.0D0
ARITH2=0.0D0
OROS1=(1.0D0+DRDTf*MACH)
OROS2=(Rf*MACH)
ARITH1=ARITH1+(1.0d0**3.d0/(Rf**3.d0+R**3.d0))**GAMA*PSTAT
ARITH1=ARITH1-2.0D0/(WEBSRBf*Rf)-4.0D0*DRDTf/(REL*Rf)
IF (TIME.LE.2.0D0*PI*PERIODSINITEND+starttime) THEN
     ARITH1=ARITH1-PINF-EINFSEC*PINF*DCOS(TIME)
ELSE
```

```fortran
    IF (TIME.GT.2.0D0*PI*PERIODSTOP-2.0D0*PI*PERIODSINITEND+starttime) THEN
        ARITH1=ARITH1-PINF-EINFSEC*PINF*DCOS(TIME)
    ELSE
        ARITH1=ARITH1-PINF-EINFSEC*PINF*Dsin(TIME)
    ENDIF
ENDIF
ARITH2=ARITH2-
(3.d0*PSTAT*GAMA*1.d0**(3*gama)/(R**3+Rf**3)**(gama+1))*(DRDT*R**2+DRDTf*Rf**2)
ARITH2=ARITH2+2.0D0*DRDTf/(WEBSRBf*Rf**2.0D0)

IF (TIME.LE.2.0D0*PI*PERIODSINITEND+starttime) THEN
    ARITH2=ARITH2+EINFSEC*PINF*DSIN(TIME)
ELSE
    IF (TIME.GT.2.0D0*PI*PERIODSTOP-2.0D0*PI*PERIODSINITEND+starttime) THEN
        ARITH2=ARITH2+EINFSEC*PINF*DSIN(TIME)
    ELSE
        ARITH2=ARITH2-EINFSEC*PINF*Dcos(TIME)
    ENDIF
ENDIF

ARITH=ARITH+OROS1*ARITH1+OROS2*ARITH2-(3.0D0/2.0D0-
DRDTf*MACH/2.0D0)*(DRDTf**2.0D0)+4.0D0*MACH*(DRDTf**2.0D0)/(REL*Rf)
PARON=PARON+(1.0D0-DRDTf*MACH)*Rf+4.0D0*MACH/REL
D2RDTFf=ARITH/PARON

END FUNCTION
```